CLAS-Note-92-008
31-March-1992

Light Readout System for the Electromagnetic Shower Calorimeter of the CEBAF Large Acceptance Spectrometer

V. Burkert[1], Yu. Efremenko[2], K. Egiyan[4]
K. Giovanetti[3], S. Stepanyan[4]

[1] CEBAF, Newport News, Virginia, USA
[2] Institute of Theoretical and Experimental Physics, Moscow, Russia
[3] James Madison University
[4] Yerevan Physics Institute, Yerevan, Armenia

Abstract

Light transmission characteristics of long scintillator strips are discussed for different readout systems. It is shown that the wavelength dependence of light transmission properties of scintillator bars has significant impact on the detector performance in the case of wavelength shifter (WLS) readout. Optical fiber light guide provide improved transparency of scintillator strips due to the reduced effective path length of light trapped in the fibers.

1. Introduction

The forward region of the CEBAF Large Acceptance Spectrometer (CLAS) [1], corresponding to scattering angles between 8^o and 45^o, will be equipped with an electromagnetic shower calorimeter (EMC). The EMC consists of six modules each covering an active region of one of the six CLAS sectors. One of the EMC modules is shown in Figure 1. Each module contains 39 layers. Each layer consists of an array of 36, 1 cm-thick approximately 10 cm wide scintillators covered by a 2.2 mm thick sheet of lead. The strips of scintillator in ach layer are rotated approximately 120^o relative to the previous layer, providing three different views (U ,V, and W) for stereo readout. The light signal from scintillators in different layers but with the same view (U, V or W) are read out together. These form stacks (36 stacks in an EMC module) that point at the target. Each stack is divided into a front segment (5 layers) and a back segment (8 layers). The light from a front segment (5 scintillators) or a back segment(8 scintillators) is collected and brought to the surface of a single photomultiplier tube. With 36 stacks, 3 stereo views and a front/back segmentation, each module will have 216 independent readout channels.

This report summarizes the results of a study of 3 light collection systems. Two of these systems, the wavelength shifter method (WLS) and the fiber method, have been proposed for use in the EMC modules. The third system, the direct method, was done for comparison.

One way to collect the light from several scintillators is to absorb the light from the end of each scintillator in a plastic light guide and then reemit this light at a longer wavelength so that a fraction of the reemitted light reaches a PMT mounted on the end. The absorption and reemission is performed by Wavelength Shifter (WLS) compounds. To readout a stack of scintillators the WLS light guides can be placed along the side of the EMC module, roughly perpendicular to a layer. This has the advantage of multiple scintillator readout in a very compact simple geometry. There are however disadvantages. There is, for example, a reduction in the number of photons due to the isotropic emission of the WLS, a degradation in timing due to the additional absorption/emission process and there are nonuniformities associated with attenuation in the WLS guides.

An alternative method for collecting the light from several scintillators is to cover a fraction of each scintillator end with optical fibers. The fibers can then be bundled at the opposite end for attachment to a cylindrical light guide and photomultiplier tube. Fibers from several scintillators can be bundled together. Plastic fibers are easily bent and so fiber light guides can be constructed that

conform to the space constraints for the EMC readout. The fibers have good transmission properties for scintillator light. However, limitations on the number of fibers that can be used and the reduced angular acceptance of the fibers with respect to that of scintillator will result in a loss of photons.

As illustrated, both methods have advantages and disadvantages. In this report the readout methods will be compared with emphasis on their impact on the measurement of the time and energy of an event in an EMC module.

2. Experimental Setup.

A schematic view of the apparatus used for testing the light readout systems is shown in Figure 2. A plastic scintillator serves as a source of light. The light can be measured using a XP2262 photomultiplier tube (PMT1) either directly coupled to the scintillator (direct readout) or coupled through the WLS or fiber systems. The scintillator light was produced by either a radioactive source, a pulse of UV light, or an 8 keV continuous x-ray source. A second photomultiplier (XP2262) tube, PMT2, served as a time reference, and as an electronic trigger. PMT2 was also used to measure the intensity of the light produced in the scintillator.

Radioactive ^{207}Bi emits a 1 MeV conversion electron. Normally most of this energy is deposited in the scintillator. These 1 MeV events can be selected using PMT2. The radioactive ^{207}Bi source could therefore be used to establish an absolute measurement of the response to a given energy, photoelectrons/MeV, for each system. In addition the radioactive source was used in determining the photon PMT arrival time distribution for each system.

A nitrogen laser was used to generate a pulse of UV light. The characteristics of the laser are given in Table I. The laser pulse was attenuated with filters and then transported to the scintillator through a quartz fiber. The UV light is absorbed and reemitted by a secondary fluor in the scintillator, thereby generating blue light. The amount of light produced in the scintillator can be varied by changing the UV pulse intensity via laser attenuation filters. The number of photons produced for any given pulse can be monitored by PMT2. The pulse duration of the UV pulse is short (300 ps) and can be used for measuring the timing characteristics of the readout systems.

Finally, the X-ray source was used to measure the apparent attenuation length of the scintillator for each readout system. Differences in the attenuation length result because the light transport characteristics of the readout systems depend on wavelength and photon angle. The DC current from PMT1 was measured as a function of the distance of the source from the end of the scintillator. The

change in the observed current vs distance from the scintillator end could be used to determine the two components in the attenuation lengths that characterized the combined scintillator/readout system.

The X-ray source, UV transport fiber and PMT2 were mounted on a moveable cart. The cart could be positioned remotely using a PC to any location along the scintillator. The whole assembly was enclosed in a 6 meter long light tight box.

Table I. Characteristics of the Nitrogen Laser.

Energy per Pulse	70 μJ
Pulse Duration	300 ps
Wavelength	337 nm
Photons per Pulse	10^{14}
Repetition Rate	1-20 Hz

3. Light Attenuation Measurements.

The scintillator bars which will be used in the calorimeter have lengths that range from 15 cm up to 460 cm. Uniform response of the EMC is important because the first level trigger of CLAS uses the summed signals of each module as a measure of total energy deposited. It is, therefore, desirable to have the minimum possible attenuation in the scintillator and light collection system.

The photons which arrive at the PMT have an energy spectrum and a distribution in angle which are determined in part by the geometry and in part by the characteristics of the materials used. For example, the emission spectrum of the scintillator (BC-412) peaks at 434 nm [4]. The longer wavelengths have better light transmission properties, such that the light traverses the scintillator a higher percentage of the blue light is lost and the peak of the spectrum shifts to longer wavelengths. A dependence on the photon angle results from the path length difference between photons that travel parallel to the scintillator and those that travel at some angle. The larger the angle the greater the path length and therefore the greater the attenuation. An average path length can be inferred from a measurement of the propagation time for a scintillator light pulse. Dividing the distance along the scintillator by this measured propagation

time an effective velocity can be defined. In the 10 cm wide 1 cm thick scintillator used for these tests an effective velocity of 16 cm/ns was obtained. This is 20% less than the actual speed of light in scintillator (19cm/ns). The average path length is 20% greater than the path which lies parallel to the scintillator. (For photons traveling at the critical angle, the path length increase is 30%). The light collection system will transmit both a modified incident spectrum as well as a modified incident angular distribution of photons, this will effect the measured attenuation length of the scintillator.

Figure 3 shows the anode current when the PMT is directly coupled to the scintillator end as a function of the position of the source along a scintillator bar (BC412 $400 \times 10 \times 1cm^3$). The end opposite to the readout was blackened to eliminate reflections. The anode current of PMT1 was measured in 5 cm increments of the position of the X-ray source from the end of the scintillator. The solid curve shows a fit to the data using a sum of two exponentials [5]:

$$A = p_1 \cdot e^{-x/p_2} + p_3 \cdot e^{-x/p_4} \tag{1}$$

Here p_1 is the amplitude and p_2 is the attenuation length for the short wavelength contribution to the measured current. p_3 and p_4 are the amplitude and attenuation length for the long wavelength contribution, respectively. Three other curves are shown for comparison. These curves were obtained using the same fitting procedure. In this measurements, filters with different cutoff wavelength were placed between the scintillator and the photocathode. The dashed curve corresponds to $\lambda \geq 420nm$ (Filter 2E), the dotted curve corresponds to $\lambda \geq 445nm$ (Filter 3) and the dash-dot curve corresponds to $\lambda \geq 475nm$ (Filter 8) (see Figure 4). A quantitative comparison of these fits can be found in Table II. The differences between the fits clearly indicate that the longer wavelengths are less attenuated than the shorter wavelengths. Thus, the effective attenuation length of a scintillator may be increased at the expense of light yield by eliminating the shorter wavelengths.

$$(p_1/p_3)_{2E} = 0.77(p_1/p_3)_0 \quad (p_4)_{2E} = 1.09(p_4)_0$$

$$(p_1/p_3)_3 = 0.51(p_1/p_3)_0 \quad (p_4)_3 = 1.22(p_4)_0$$

$$(p_1/p_3)_8 = 0.46(p_1/p_3)_0 \quad (p_4)_8 = 1.5(p_4)_0$$

where index "0" means fitting parameters without filters.

When wavelength shifters are used for readout, the measured attenuation length of the scintillator is changed as well. The wavelength shifters have absorption and emission probabilities that depend on the wavelength. This can be seen by examining the absorption spectra of BC499 and BC482 WLS shown in figure 5. The dashed line is the emission spectrum of BC412 scintillator. The WLS are most sensitive to short wavelengths, thereby effectively selecting the region of the scintillator spectrum with shorter attenuation length. We have measured the attenuation length of the scintillator for light collected with four different WLS: G2, BC482, BC499 and NE172. For these measurements the WLS was placed perpendicular to the scintillator with a 1 mm air gap. In Figures 6 we show the measured data and results of fitting. The fitting function was the same as above and is given in equation 1. The dashed lines in figure 6 show the fits to measurements where the PMT was directly coupled to the scintillator. The effective attenuation length (p_4) measured with WLS was always smaller than in the case of direct coupling. Also the ratio $\frac{p_1}{p_3}$ increased for the WLS's, indicating an increase of the shorter wavelength compounds for the light seen by the PMT.

In the case of optical fibers, the spectrum of light exiting the scintillator is transported unchanged to the PMT. The fibers are connected so that the fiber axis is perpendicular to the scintillator end. A few centimeters after the connection the fibers are bent through 90^o with a radius of curvature of 1.2 cm. Theses fibers are eventually brought together in a cylindrical bundle that is attached to a lucite rod which fits onto the cathode of the PMT (Figure 2).

One important feature of the fiber readout is that the fibers reduce the angular divergence of the light. They select rays which have an angle of less than 20^o with respect to the axis. This angle is determined by the ratio of the index of refraction of the fiber core to that of the fiber cladding. The angular acceptance of the fiber is smaller than the angular transmittance of the scintillator. Approximately 28% of the incident light is transmitted by the fibers. By only accepting the photons which have small angles with respect to the scintillator transmission axis, photons that travel short path lengths and suffer fewer reflections from the scintillator surface are selected. The result is an increase in the effective attenuation length with the fiber readout system.

In Figure 7, the results of attenuation measurement using a 2 mm diameter plastic optical fibers with polystyrene core and PMMA clad are presented. The data were fitted to the given expression in equation 1. The attenuation length has significantly increased. Parameter p_4 is $\sim$ 15% grater than what it was measured using direct coupling (solid curve).

Results of measurements with fiber readout system combined with wavelength selective filters placed in front of the PMT are shown in figure 8. The filters used were the same as those discussed above for the direct readout case. The solid line is a fit to the data when no filters are used. The dashed curve is a fit to data measured when filter 2E was used. The dotted curve is a fit to data obtained with filter 3.

The results of the attenuation measurements are summarized in table II. The direct coupling represents the upper limit for the attenuation performance of a WLS readout. This limit can only be attained when the scintillator emission and WLS absorption spectra are identical. However this matching is never perfect. A shorter attenuation length is therefore observed when WLS readout is used. For optical fibers, an increases in the effective attenuation length is observed. Also included in the table are the measurements which give the greatest attenuation lengths. These were obtained by combining the optical fiber readout with wavelength selective filters.

Table II. Attenuation performance of 4.m long BC412 scintillator at various type of readout system.

Light Readout	$\frac{p_1}{p_3}$	p_2	p_4
Direct Joint PMT	0.54 ± 0.003	$47. \pm 0.7$	$274. \pm 0.9$
WLS G2	1.26 ± 0.008	$28. \pm 0.1$	$186. \pm 0.5$
WLS BC482	0.92 ± 0.009	$34. \pm 0.4$	$206. \pm 1.1$
WLS BC499	0.87 ± 0.007	$33. \pm 0.8$	$221. \pm 1.1$
WLS NE172	0.96 ± 0.006	$28. \pm 0.3$	$220. \pm 0.6$
Optical Fibers	0.4 ± 0.006	$52. \pm 1.3$	$326. \pm 2.1$
Optical Fibers Filter "2E"	0.25 ± 0.007	$42. \pm 0.8$	$341. \pm 0.7$
Optical Fibers Filter "3"	0.2 ± 0.005	$30. \pm 0.8$	$383. \pm 0.8$

4. Absolute Light Yield.

To measure the absolute light yield a ^{207}Bi source was used. The source was centered along the scintillator width at a position 10 cm from the readout end. PMT2 was placed directly opposite the source (Figure 2). Figure 9 shows a pulse height spectrum that was measured using PMT2. The peak is due to 1 MeV conversion electrons. The spectrum of PMT1 that corresponds to this 1 MeV peak in PMT2 could be analyzed to determine the systems response to an energy deposition of 1 MeV. In order to find the average number of photoelectrons for this spectrum the data was fitted to a sum of Gaussians, which described the response of the photomultiplier to a fixed number n_{pe} of photoelectrons. The centroid of each Gaussian should be proportional to n_{pe}, while the width of these Gaussians should increase with $\sqrt{n_{pe}}$. Two parameters, a_1 and a_0, are used to establish the relationship between ADC channel number and number of photoelectrons. The fitted parameter a_1 represents the centroid for the single photoelectron events and σ_1 is determined by the width of the single photoelectron peak (Figure 10). The fitted parameter a_0 represents the difference between the centroids of two adjacent gaussian. For a given energy deposition in the scintillator the actual number of photoelectrons at PMT1 follows a poisson distribution. This distribution will depend on the average number of photoelectrons. The Gaussians in the summation were therefore weighted by a Poisson distribution. The complete function used to fit the PMT1 spectrum is given in equations 4, 5 and 6 below.

$$A = C \cdot \sum P_i(n_{pe}) \cdot G_i(n_{ch}) \tag{4}$$

where

$$P_i(n_{pe}) = \frac{n_{pe}^i \cdot e^{-n_{pe}}}{i!} \tag{5}$$

and

$$G_i(n_{ch}) = \frac{1.}{\sigma_1 \cdot \sqrt{i}} \cdot e^{-\left(\frac{n_{ch} - (a_1 + (i-1)\cdot a_0)}{2. \cdot \sigma_1 \cdot \sqrt{i}}\right)^2}, \tag{6}$$

where, n_{pe} is the average number of photoelectrons and n_{ch} is the actual ADC channel number, respectively. The parameter C provided an overall normalization. The summation was carried out over the variable i, which represents possible values for the number of photoelectrons.

For a fixed high voltage on PMT1 the parameters a_1, σ_1 and a_0 were expected to remain constant. This was verified by fitting several spectra. The parameters

a_1 and σ_1 were obtained from single photoelectron spectra of PMT1. The parameters were then fixed to their average value from several fits to the few photoelectron data. This analysis of several spectra yielded $a_0 \simeq 0.95 \cdot a_1$. This is interpreted to mean that the mean value for the zero photoelectron peak was slightly higher than the pedestal.

There was a substantial increase in the number of photoelectrons when PMT1 was coupled directly to the end of the scintillator. In this case a single Gaussian was used to fit the spectrum and the number of photoelectrons was determined using

$$n_{pe} = \frac{A_G - a_1}{a_0} + 1 \tag{7}$$

where A_G is the centroid parameter for the gaussian. A correction was made to account for the fact that only part of the scintillator was used. The photocathode surface only overlapped 44% of the scintillator end. The parameter n_{tot} represents the total number of photoelectrons for complete coverage of the scintillator end. The value obtained for this parameter is:

$$n_{tot} = \frac{n_{pe}}{0.44} \simeq 200 pe/MeV.$$

Figure 11 show 1 MeV pulse height spectra for the WLS readout with wavelength shifters G2, BC482, BC499, and NE172. The solid lines represent fits using the function described in (4). Similar spectra are shown in Figure 12 for the fiber readout system. The fiber bundle consisted of 60 2mm diameter plastic fibers. The fibers covered 18% of the area of the scintillator end. The fibers were bent through an angle of 90^o. The radius of curvature for the bend was 1.2 cm

The data are summarized in the Table III. The absolute light output for the various readout systems is given.

Table III. Absolute light yield from BC412 scintillator
for various type of readout systems.

Light Readout	n_{pe}/MeV	χ^2
WLS G2 †	6.1 ± 0.03	1.44
WLS BC482 †	7.8 ± 0.04	1.073
WLS BC499 †	6.8 ± 0.04	1.012
WLS NE172 †	7.6 ± 0.04	1.141
Optical Fibers readout 18% light output area	8.4 ± 0.05	1.12

† Scintillator end on 10cm from shifter-light guide gluing point

It is clear that there are a limited number of photoelectrons for WLS system. This is due in large part to the inability of the WLS to transport most of the isotropically emitted light to the PMT and to the decreased sensitivity of photocathode to green light (Q.E. at 510nm $\simeq$ 10%). BC482 had the highest number of photoelectrons per MeV with $n_{pe} = 7.8/MeV$.

The EMC detector will have several scintillators illuminating the same PMT. In the fiber readout system this is accomplished by bundling the fibers from several scintillators together. The maximum number of optical fibers that can be used to readout a scintillator will be restricted by the total number of fibers which will fit on the photocathode surface of a PMT and to area on scintillator. The active photocathode area for 2" PMT's is $\sim 1500.mm^2$. In the back EMC segment a PMT will readout 8 scintillator bars. Each scintillator can illuminate only 1/8 or $\sim 180mm^2$ of the available photocathode. This limits the scintillator end coverage to approximately 18%. As mentioned, the fiber system tested satisfied this restriction in scintillator coverage. The number of photoelectrons under these conditions is comparable to the WLS methods with $n_{pe} = 8.4/MeV$. It should be noted that a light guide with an area larger than the active photocathode could be used. The optical fibers transmit a smaller

angular range of light than a plastic light guide. A cone shaped light guide could be used to compress the cross sectional area of the light from a fiber bundle. Area compression produces angular expansion (phase space conservation) but because the light guide will transmit a larger angular range than the fiber all the light can still be transmitted to the PMT.

5. Time Characteristics.

The electromagnetic shower calorimeter, EMC, will be the most sensitive of the CLAS detectors to neutrons. When a neutron collides with a nucleus some of the neutron energy can be transmitted to particles that are easily detected by the EMC detector. A measured time and a deposited energy can then be determined for those neutrons that interact in the detector. The energy deposition is typically not sufficiently correlated to the incident neutron energy to be used as a measure of the incident neutron energy. The *time of flight* (TOF) of the neutrons from the target to the calorimeter is usually a more accurate way to determine neutron energies /7/. The timing characteristics of the EMC detector will therefore be important.

Time resolution is limited by fluctuations in the light collection time, by photoelectron statistic and by the timing characteristics of the PMT [7]. Each of the readout system will have different timing properties. In order to study these properties several tests were performed.

The fluctuations in light collection time are largely determined by the absorption, emission and transmission processes that occur in the scintillator and the readout system. In order to measure these effects the signal on the PMT was attenuated to the point where no more than one photon would be present. The normalized time spectra that were recorded under these conditions can be interpreted as the probability of photon arrival versus time. Because the whole photocathode was used in these measurements the jitter in transit time due to differences in the position of the photon on the photocathode, 700 psec, also influenced the measurement.

The time spectra shown in Figures 13 and 14 were taken using the single photoelectron technique described above. After the intial rise the number of events falls off exponentially in time.

$$N_{ev} = C \cdot e^{-\frac{t}{\tau_0}} \tag{8}$$

The falloff can be characterized by the single parameter τ_o. This parameter, referred to as the decay time, is dominated by the slowest process. For the case of the PMT directly coupled to the scintillator, a fit of the spectrum using (8) found $\tau_0 = 3.8ns$. This value is slightly larger than the known value ($\tau = 3.6ns$) for the decay time of BC412 scintillator. This is due, at least in part, to the time resolution of trigger PMT2 (small photoelectron statistics).

The corresponding spectra for the G2, BC482, BC499 and NE172 WLS readouts are shown in Figure 14. The fitted values for τ_0 ($\tau_0 = 5.1ns$ for G2, 8.7ns - BC482, 7.4ns - BC499 and 6.1 - NE172) are larger than the direct coupled case. This is due to the wavelength shifting fluor which absorbs and reemits the scintillator light in the WLS. This increase will not significantly influence the time characteristics if there are sufficient numbers of photoelectrons. However, if only small amount of energy is deposited in each of the three views (U, V, W) the decay time of the readout system can seriously limit the time resolution.

The time resolution was measured as a function of the number of photoelectrons and as a function of the position where the light was injected into the scintillator. Scintillator light was generated with a pulse of UV light. The UV pulse was delivered by an optical fiber which was confined to a small region of the scintillator. The amount of UV light could be varied and the fiber that delivered the UV light could be positioned at any location along the scintillator. PMT2 moved with the UV source fiber and was used to measure the amount of scintillator light that was generated. By comparing the response of PMT2 for the UV source with the response to the known energy deposition of the ^{207}Bi source an absolute calibration in terms of both energy and photoelectrons could be made. For a definite position of the UV fiber and a fixed attenuation in the UV delivery system a time and amplitude spectrum for PMT1 was recorded. These spectra were corrected for the pulse to pulse changes in UV intensity. The time resolution and the energy resolution were determined from the corrected spectra by fitting the peaks to Gaussian distributions.

Figure 15 shows a comparison of the time resolution between the NE172 WLS (filled) readout and the fiber readout (open) system for both 10 MeV (squares) and 20 MeV (triangles) of deposited energy. For both systems the time resolution improves with increasing energy deposition. The improved time resolution of the fiber system is also apparent. The poorer time resolution of the WLS system is due to a combination of longer decay time and reduced attenuation length. The solid lines represent a fit of the data using the function $\sigma_t = C \cdot e^{(-X/\sigma_0)}$.

6. Time and Amplitude Resolution for the Optical Fiber Readout.

A full range of UV intensities and UV fiber positions was recorded and analyzed for the fiber readout. Figure 16 summarizes the time resolutions obtained from these studies. The measurements correspond to equivalent energy depositions of 10 MeV, 20 MeV, 50 MeV, 77 MeV, 113 MeV and 150 MeV. The curves are results of fits to the data using the function:

$$\sigma_t = \sqrt{a^2 + \frac{b^2}{n_{pe}}} \tag{9}$$

The solid line is a fit to all data taken at the 10 cm position. The dashed line is a fit to all data recorded at the 360 cm position. The dominant feature of this data is the broadening in the time resolution with decreasing average photoelectron number. The worsening of the time resolution (solid vs dashed) for a fixed number of photoelectrons but a longer path through the scintillator is also evident.

Figure 17 shows the dependence of the parameters a and b on the distance X from the scintillator end. The difference in photon arrival time caused by a differences in photon flight path are amplified as the distance X increases. a and b can both be seen to increase with X. The solid curves represent fits to the exponential functions [X(cm)]:

$$a = 0.041 \times e^{(0.003X)}$$

$$b = 2.575 \times e^{(0.0007X)}$$

A similar analysis can be performed on the amplitude spectra. First the data are corrected for fluctuations in the UV pulse intensity. A given spectrum then corresponds to the response of the scintillator and readout system to a fixed amount of deposited energy. The amplitude resolution $\frac{\sigma_A}{A}$ can be determined by fitting each spectrum to a gaussian distribution, where A is the amplitude and σ_A is the width. The results of these fits are summarized in figure 18. These resolutions can be characterized by the parameters a and b using an expression similar to (9)

$$\frac{\sigma_A}{A} = \sqrt{0.084^2 + \frac{1.05^2}{n_{pe}}}$$

For the amplitude resolution the parameters a and b, as expected, do not show any significant dependence on X.

7. Conclusion.

Scintillator readout with an optical fiber system has been shown to have a better time resolution and a longer attenuation length than scintillator readout with WLS.

In addition, the fiber system gives a more uniform response for all scintillators in a segment (common PMT). The WLS readout attenuates the light from the scintillators close to the PMT less than for those far from the PMT. The light yield from different strips will depend on the position of the particular strip along the WLS. The result is a variation in the detector response as a function of depth of the energy deposition. This variation can be compensated for by masking the scintillator near the PMT in such a way as to correct for the attenuation in the WLS. However, this can only be achieved at the expense of additional reduction of the light yield. The long attenuation lengths of 2 mm diameter polystyrene fibers is ($\sim 0.2db/m$) makes the difference in the light loss for 30 cm versus 70 cm length fibers negligible. The fiber system therefore maintains a much more uniform response for all scintillators.

In summary, the optical fiber readout system is clearly superior to the WLS readout.

Acknowledgements.

We are grateful to Randy Wojcik for making computer software available to us and for preparing the light tight box. We also wish to thank Stan Majewski, Elton Smith and Carl Zorn for useful discussions and help during the measurement.

Figure 1. Sketch of one of six CLAS electromagnetic calorimeter modules.

Figure 2. Schematic outline of test setup.

Figure 3. Attenuation of light along 4.m long BC412 scintillator strip in the direct joint PMT. $\times$ - direct measurement, dashed line - used filter No."2E" between photocathode and scintillator end, doted - filter No."3", dashed-doted - filter No."8".

Figure 4. Emission spectra of BC412 (dashed line) with transmission spectrum of "2E" (star) and "3" (cross) filters.

Figure 5. Emission spectra of BC412 (dashed line) with transmission spectrum of BC482 and BC499 WLS's.

Figure 6. Dependence of light yield from distance along 4.m long BC412 scintillator bar, when light was readout through the G2, BC482, BC49 and NE172 WLS. Dashed line is direct joint PMT case.

Figure 7. The same as a on Figure 6 for the 2.mm diameter plastic fibers light quid.

Figure 8. The same as a on Figure 7 (solid line), dashed line - was used filter "2E" and doted - filter "3".

Figure 9. Spectra of trigger PMT for the ^{207}Bi source. Right peak correspond to 1.MeV electrons.

Figure 10. Single photoelectron peak of PMT1. Curve is Gaussian fit of peak.

Figure 11. Absolute light yield correspond to the 1.MeV energy deposition in the BC412 scintillator in the WLS readout case. ^{207}Bi source was released on 10.cm far from readout end of scintillator, while position of scintillator was on 10.cm from *WLS - Lucite Light Guide* gluing point. Curve correspond to the fit by (4).

Figure 12. Absolute light yield correspond to the 1.MeV energy deposition in the BC412 scintillator in the optical fiber readout case.

Figure 13. Time distribution of BC412 scintillator light.

Figure 14. Time distribution of G2, BC482, BC499 and NE172 wavelength shifters emitting light.

Figure 15. Dependence of time resolution of EMC via distance from readout end WLS (fill) and optical fiber (open) readout case for the 10 MeV (square) and 20 MeV (triangle) energy deposition in the single view (U,V or W) of front part.

Figure 16. Dependence of σ_t via number of photoelectrons for the 10 MeV, 20 MeV, 50 MeV, 77 MeV, 113 MeV and 150 MeV energy deposition in the different distance from readout end of front layer (open circle - 10.cm, open square - 60.cm,fill square - 110.cm, open triangle - 160.cm, open diamond - 210. cm, open cross - 260.cm, fill star - 310.cm and asterisk - 360.cm). Solid line correspond to the fit by (9) data for the 10.cm and dashed is 360.cm one.

Figure 17. Dependence of fitting parameters a and b in (9) from distance. Curves are fit by exponent.
Figure 18. The same as a in Figure 16 for the amplitude resolution (σ_A/A).
Figure 19. The same as a in Figure 17 for the σ_A/A fit by (9).

References

[1] CEBAF Conceptual Design Report - Basic Experimental Equipment, April 1990.

[2] R.Bolton at al. "A ^{207}Bi Light Pulser for Stabilization of Scintillation and Lead Glass Cherenkov Detectors", NIM 174, 1980, pp.411-419.

[3] PRA Nitrogen Laser LN120C. PRA LASER INC.

[4] Bicron Handbook. Bicron corporation, 1990

[5] V.Burkert at al. "Plastic Scintillator and Wavelength Shifter tests for the CLAS Electromagnetic Calorimeter ", CLAS-Note-91-005, March 6,1991.

[6] Photomultipliers Data Handbook. Philips, 1990

[7] Conceptual Design Report Basic Experimental Equipment, CEBAF, 1990

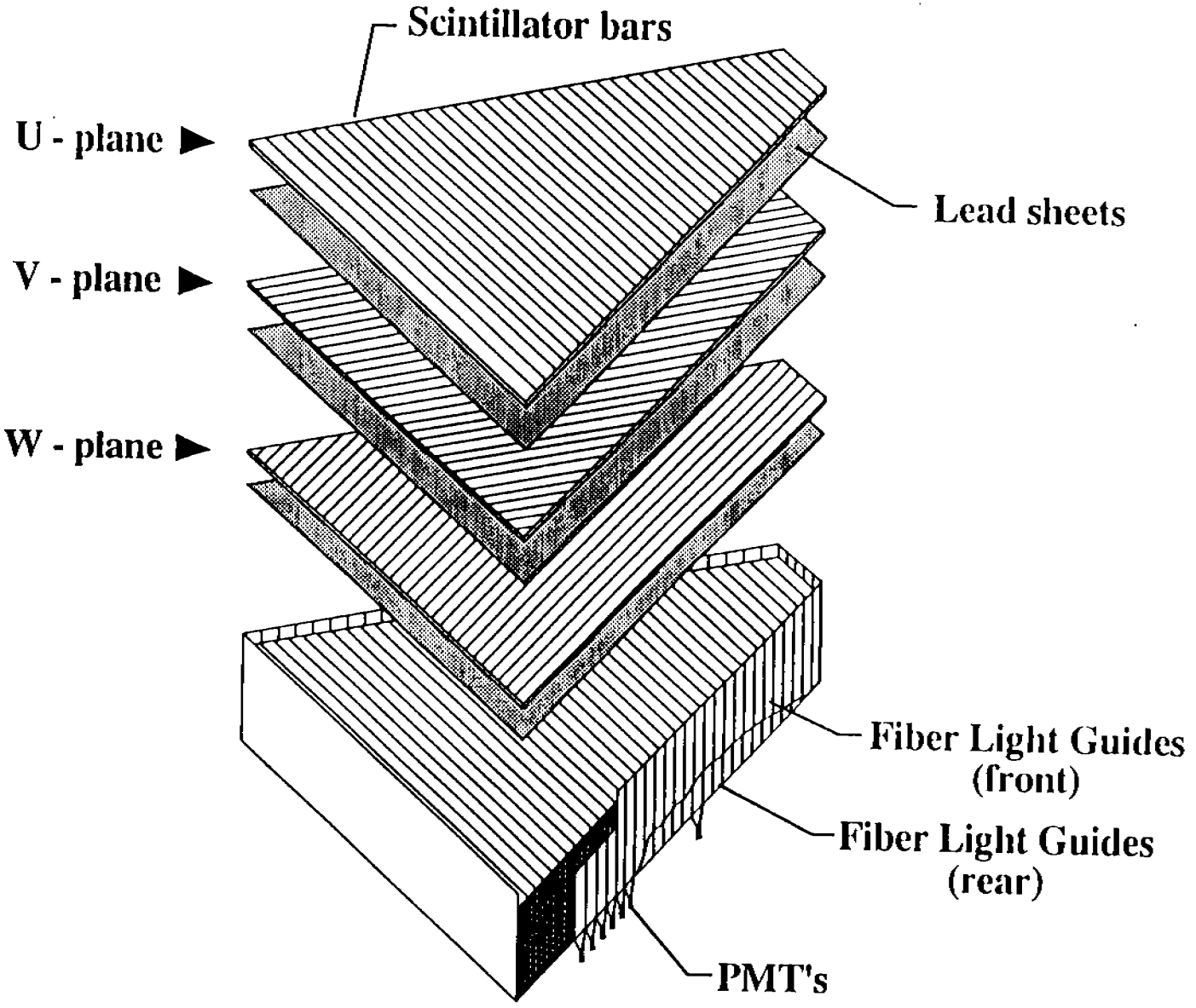
Scintillator bars
U - plane
V - plane
W - plane
Lead sheets
Fiber Light Guides
(front)
Fiber Light Guides
(rear)
PMT's

Figure 1.

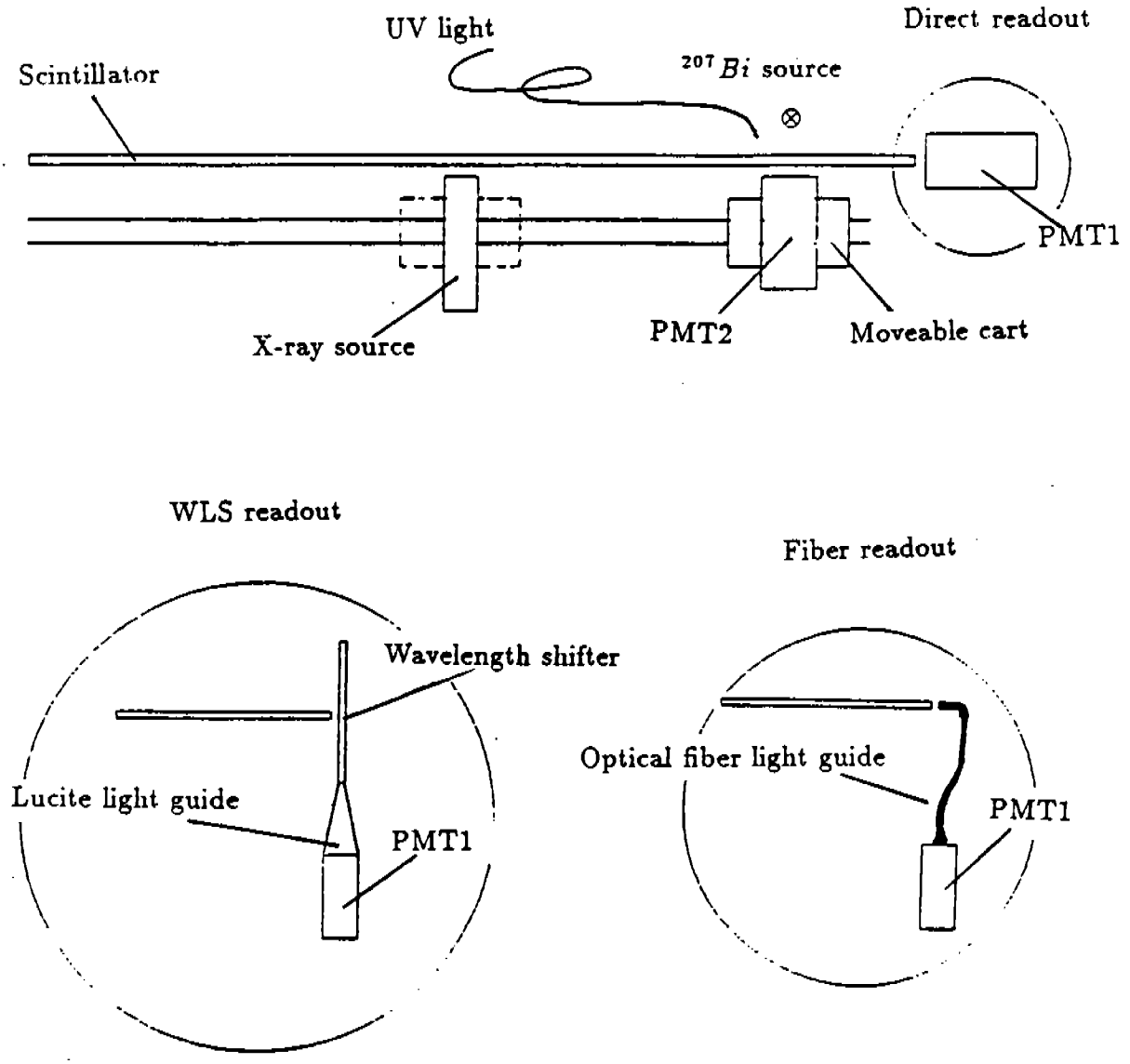
UV light
Direct readout
Scintillator
^{207}Bi source
PMT1
X-ray source
PMT2
Moveable cart
WLS readout
Fiber readout
Wavelength shifter
Optical fiber light guide
Lucite light guide
PMT1
PMT1

Figure 2.

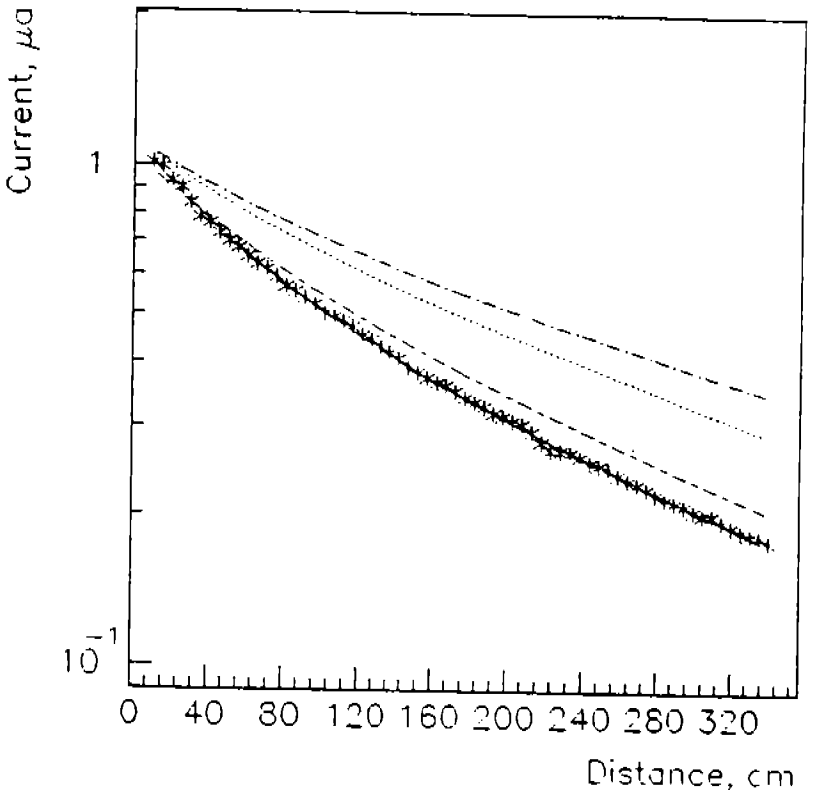

Figure 3

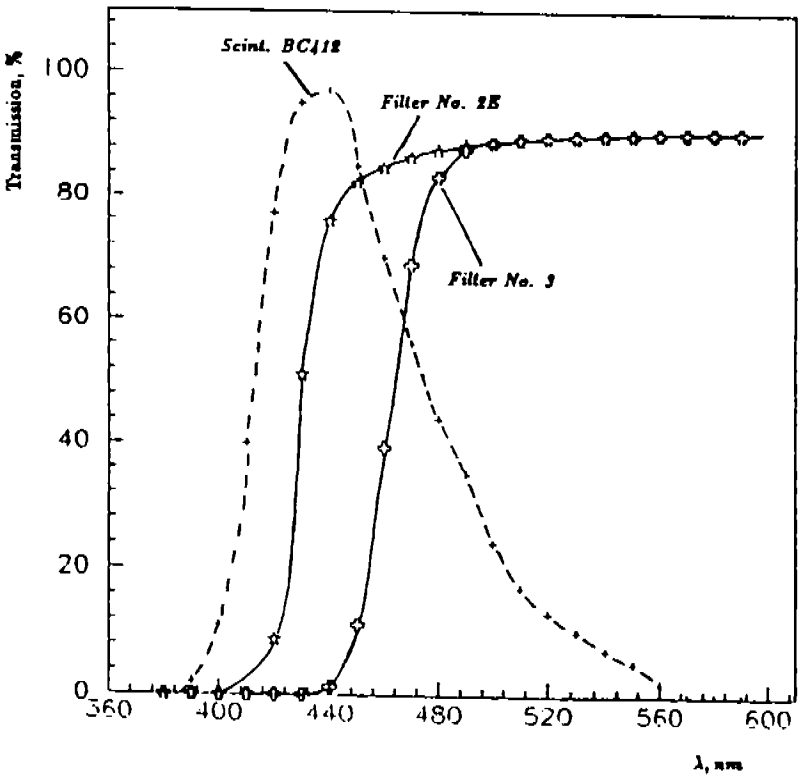

Figure 4

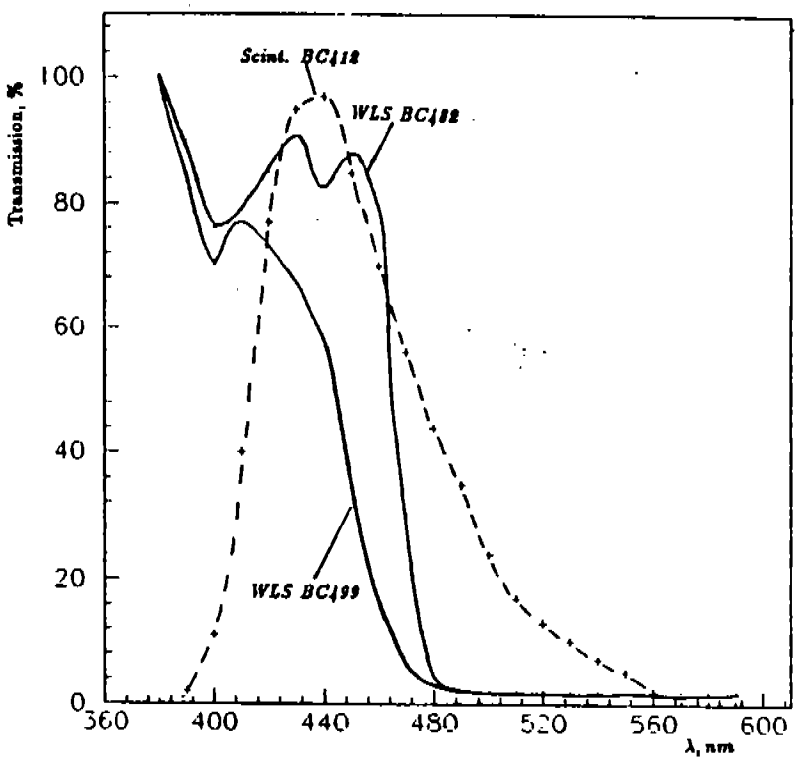
Scint. BC418
WLS BC482
WLS BC499
Transmission, %
100
80
60
40
20
0
360
400
440
480
520
560
600
λ, nm

Figure 5

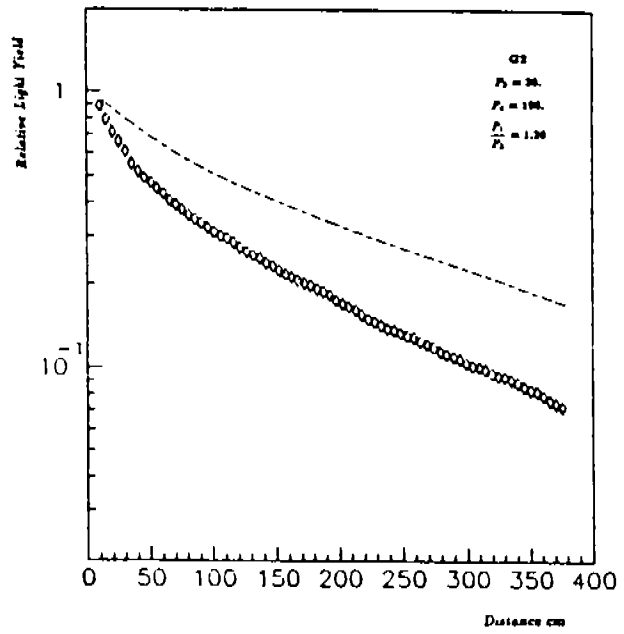
Relative Light Yield
1
10^{-1}
0 50 100 150 200 250 300 350 400
Distance cm

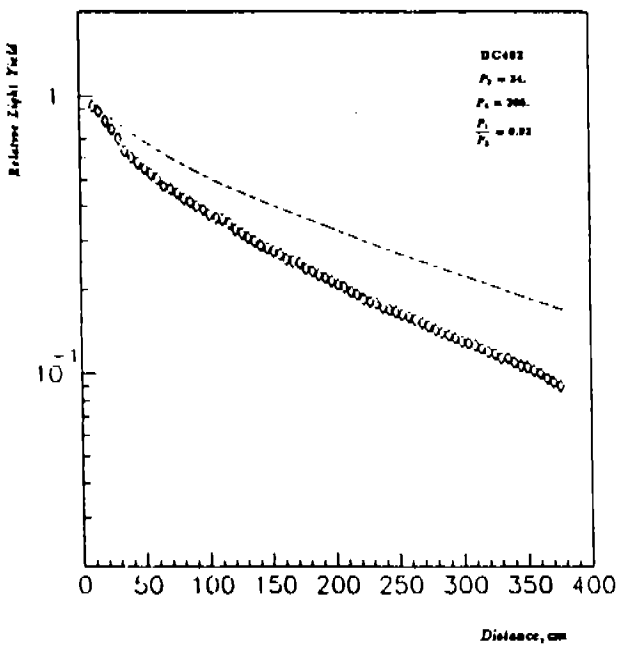
Relative Light Yield
1
10^{-1}
0 50 100 150 200 250 300 350 400
Distance, cm

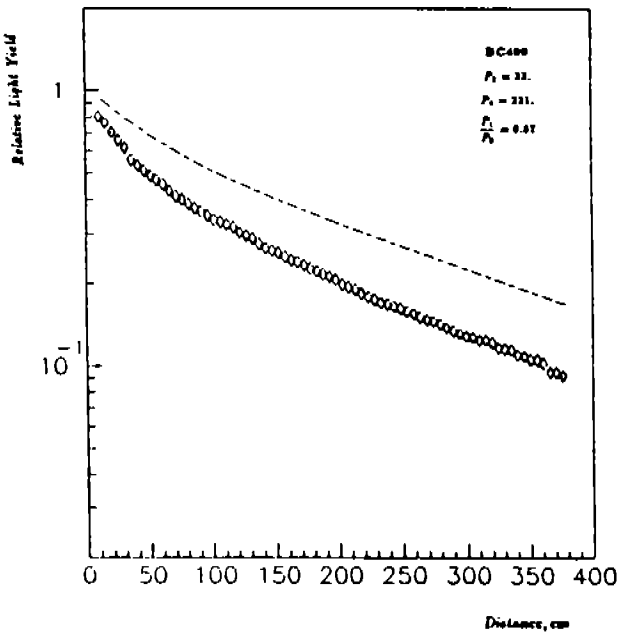
Relative Light Yield
1
10^{-1}
0 50 100 150 200 250 300 350 400
Distance, cm

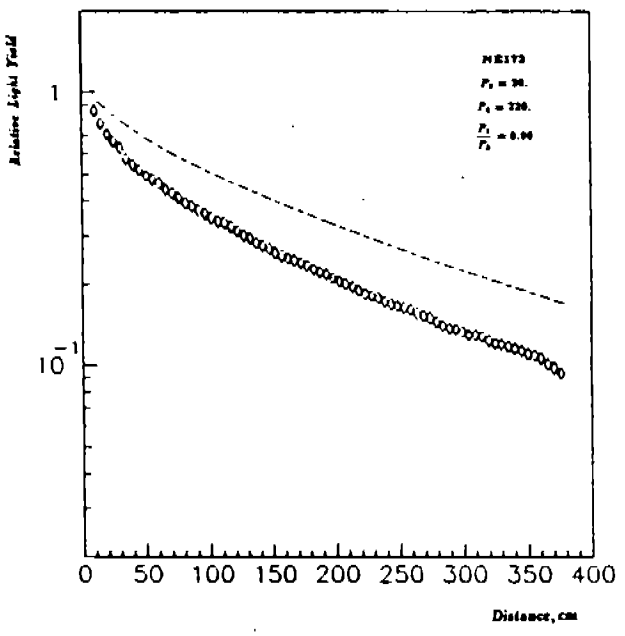
Relative Light Yield
1
10^{-1}
0 50 100 150 200 250 300 350 400
Distance, cm

Figure 6

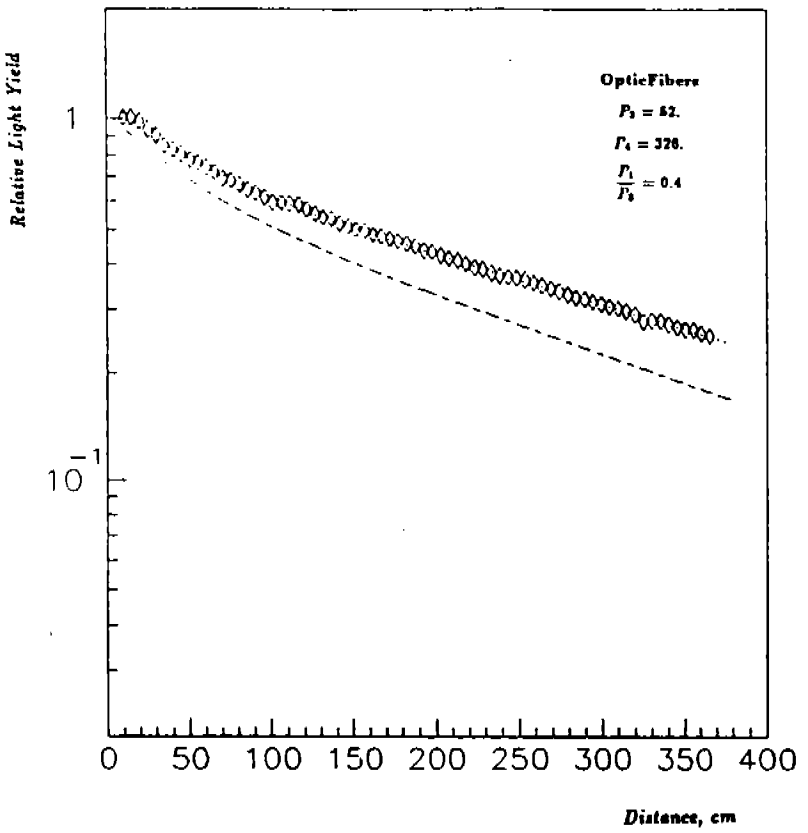

Figure 7

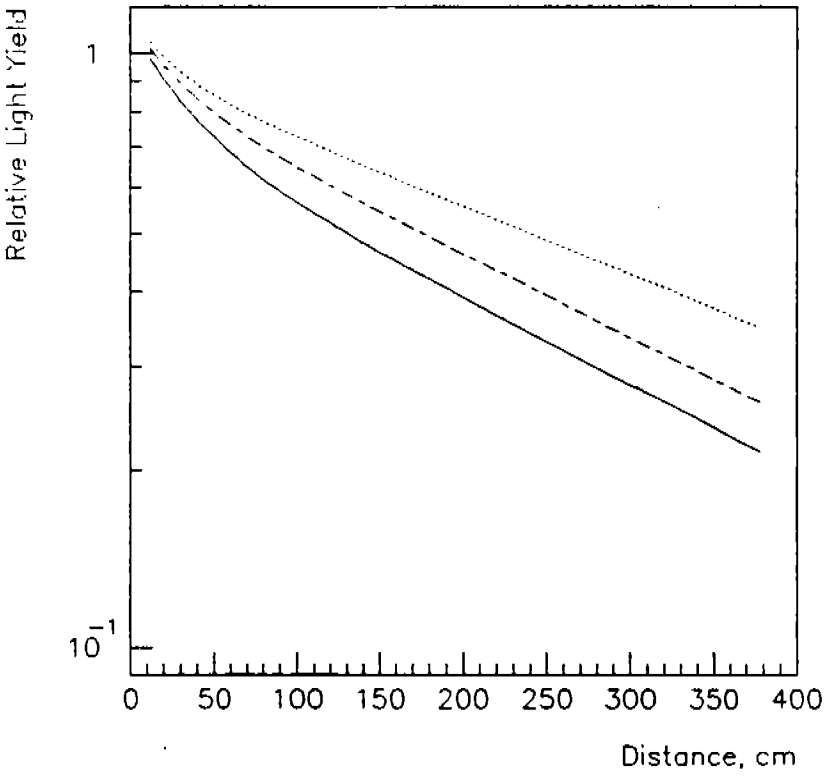

Figure 8

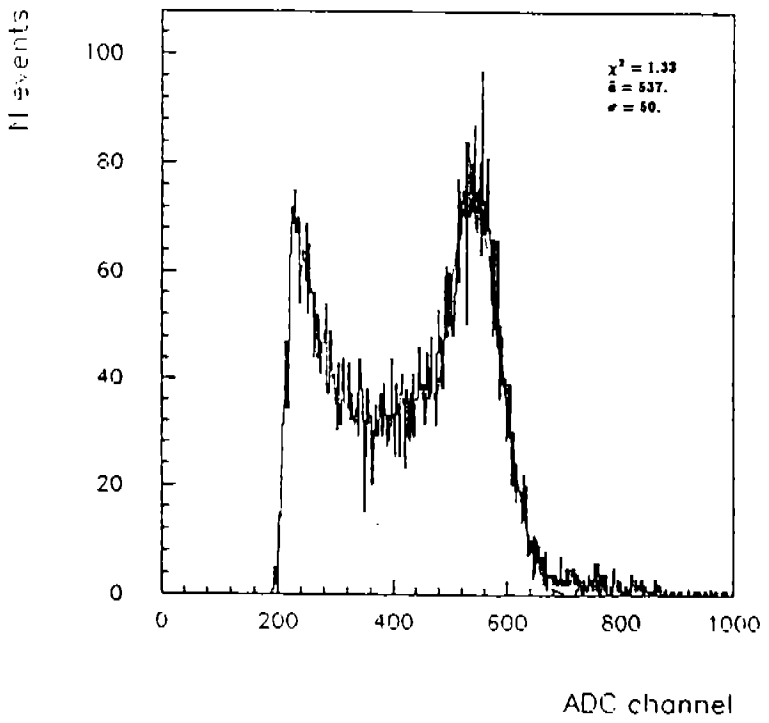

Figure 9

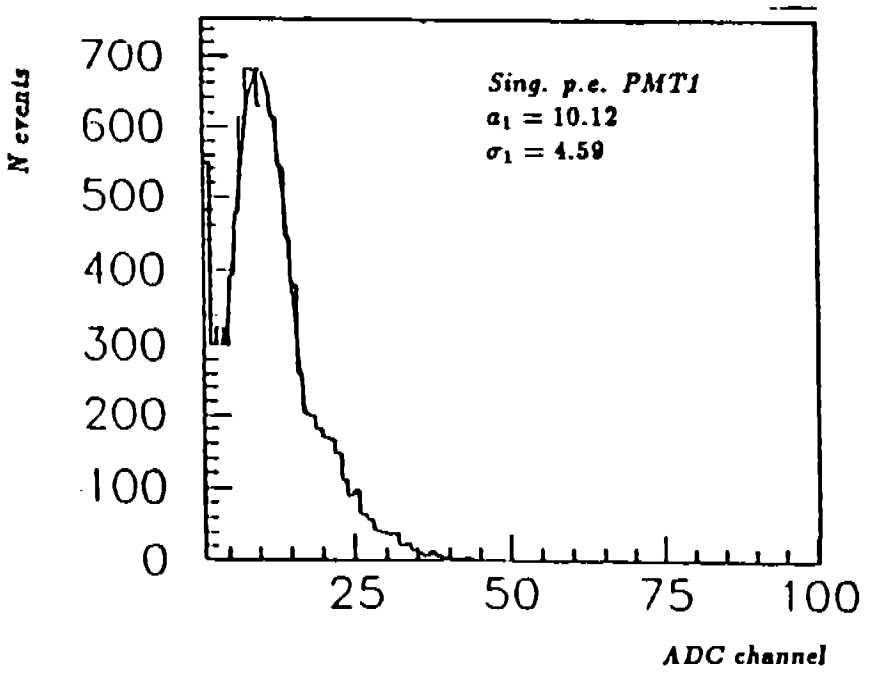

Figure 10

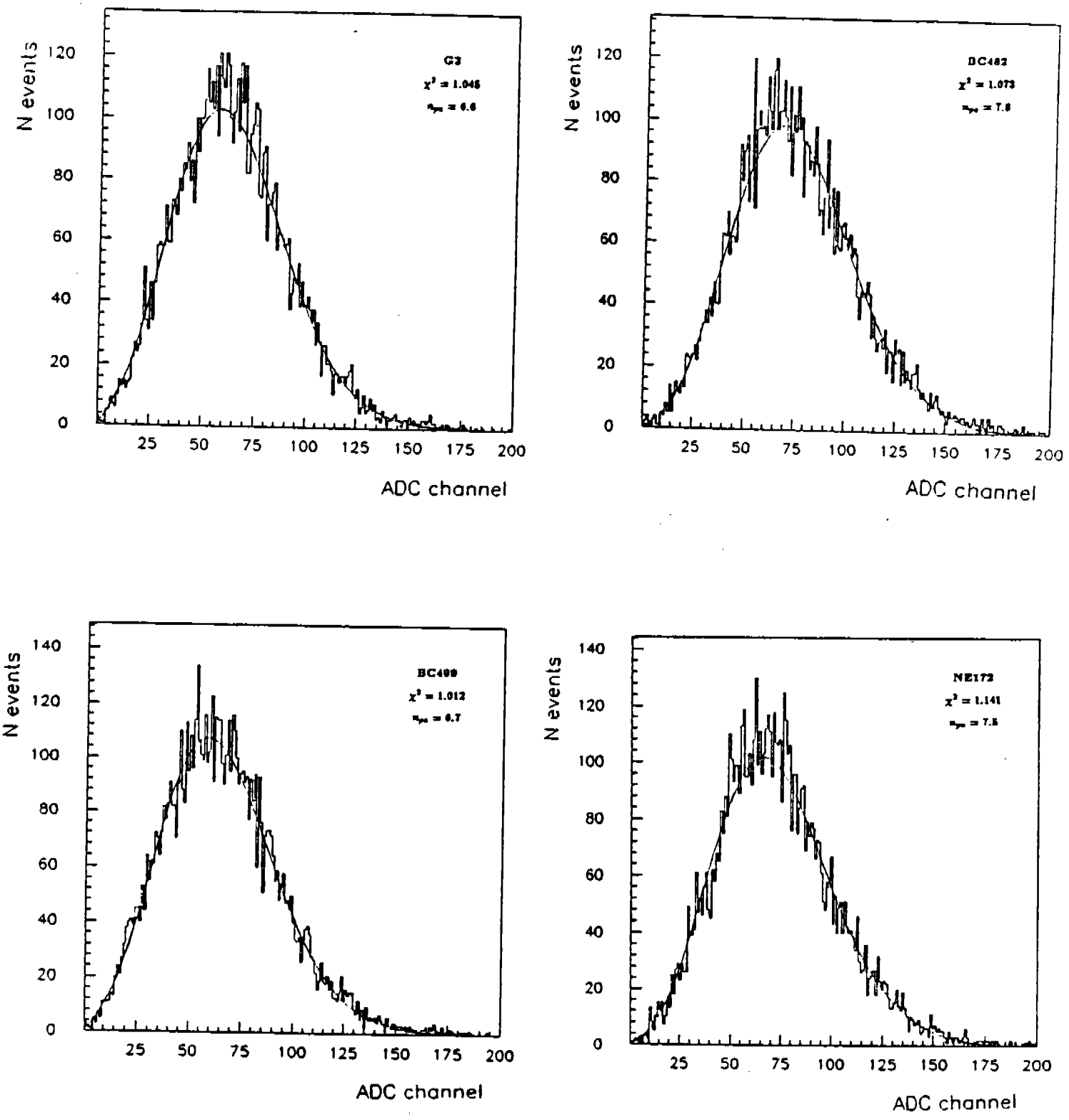

Figure 11

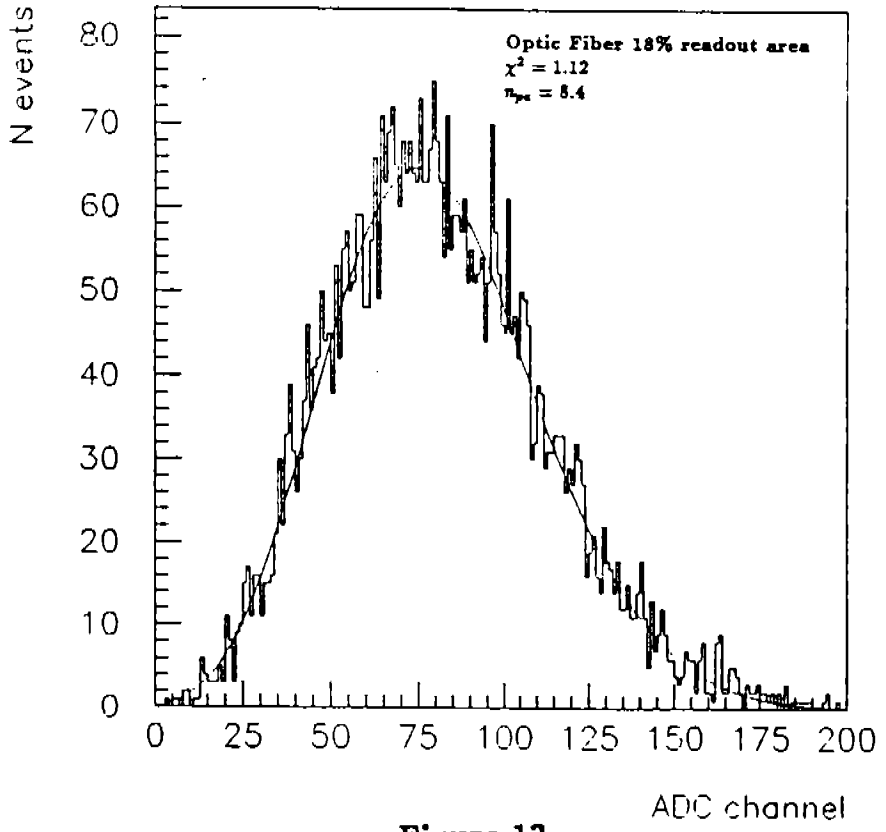

Figure 12

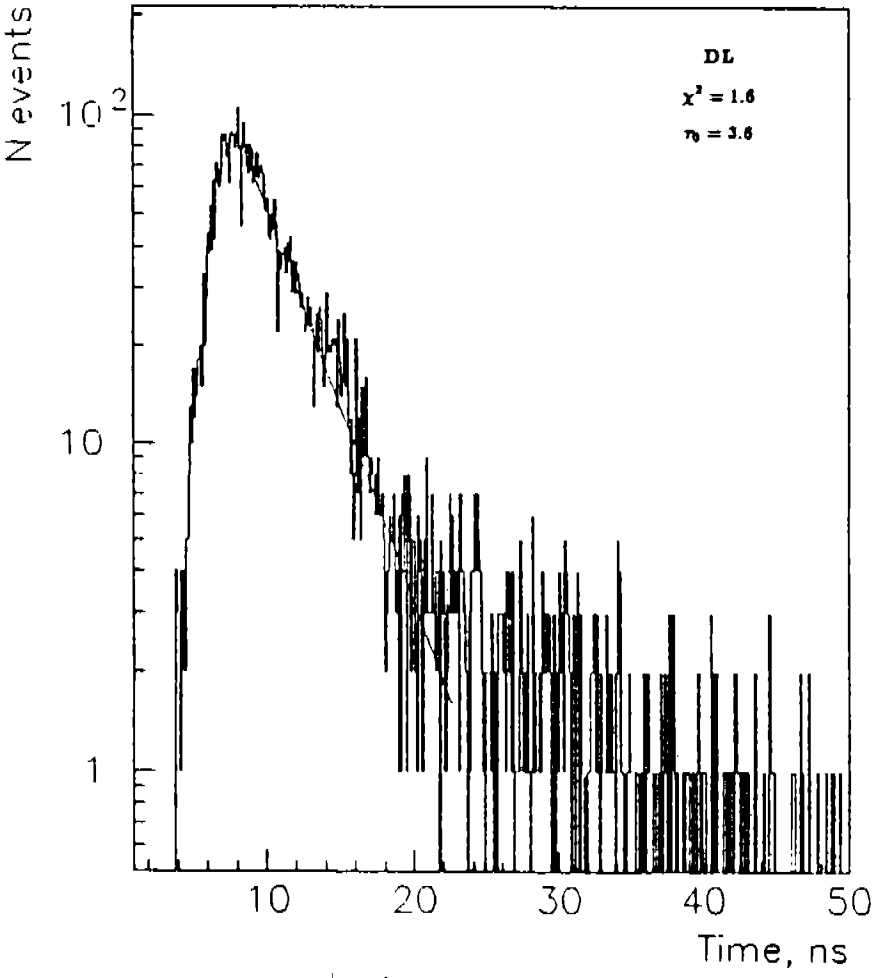

Figure 13

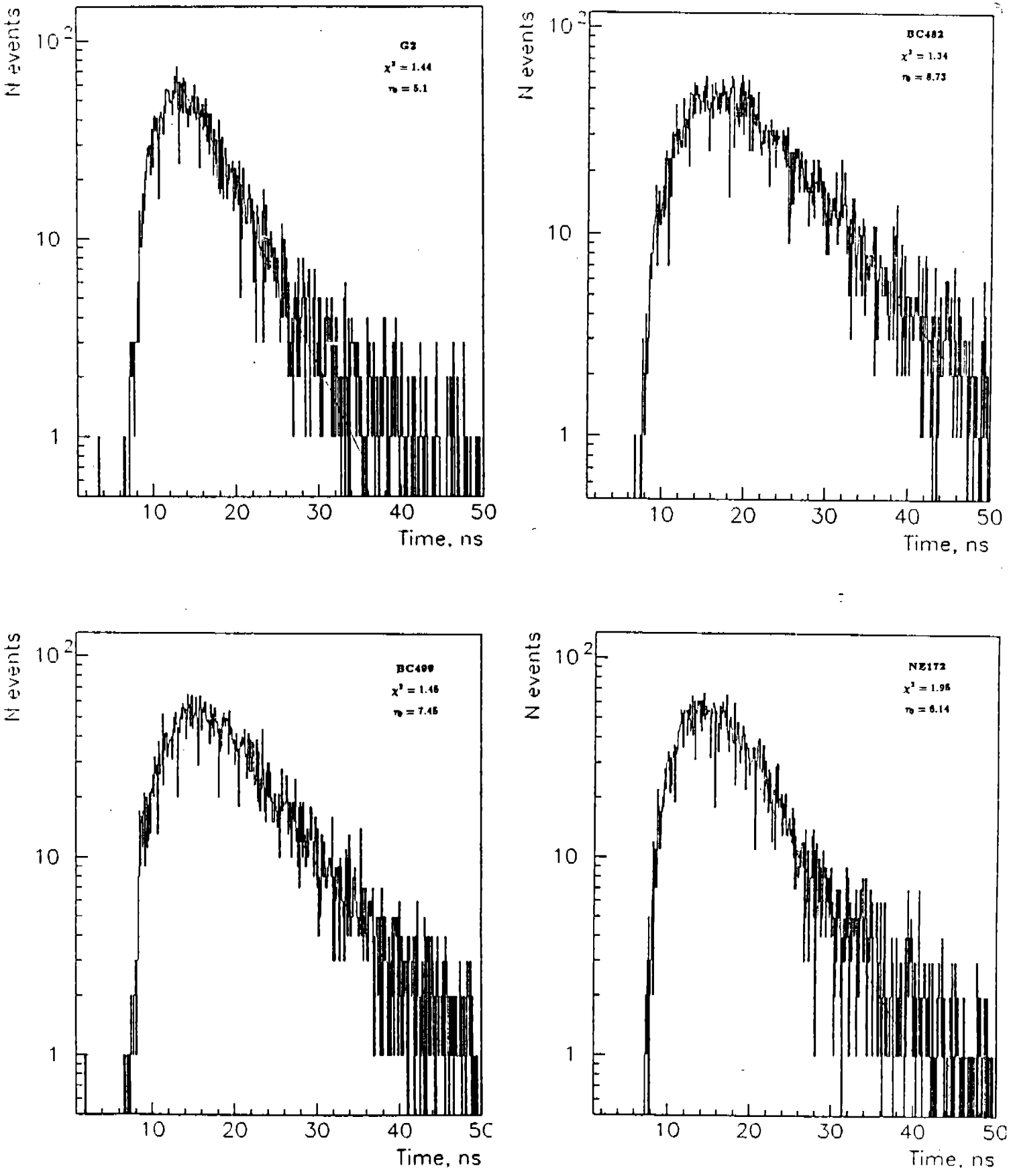

Figure 14

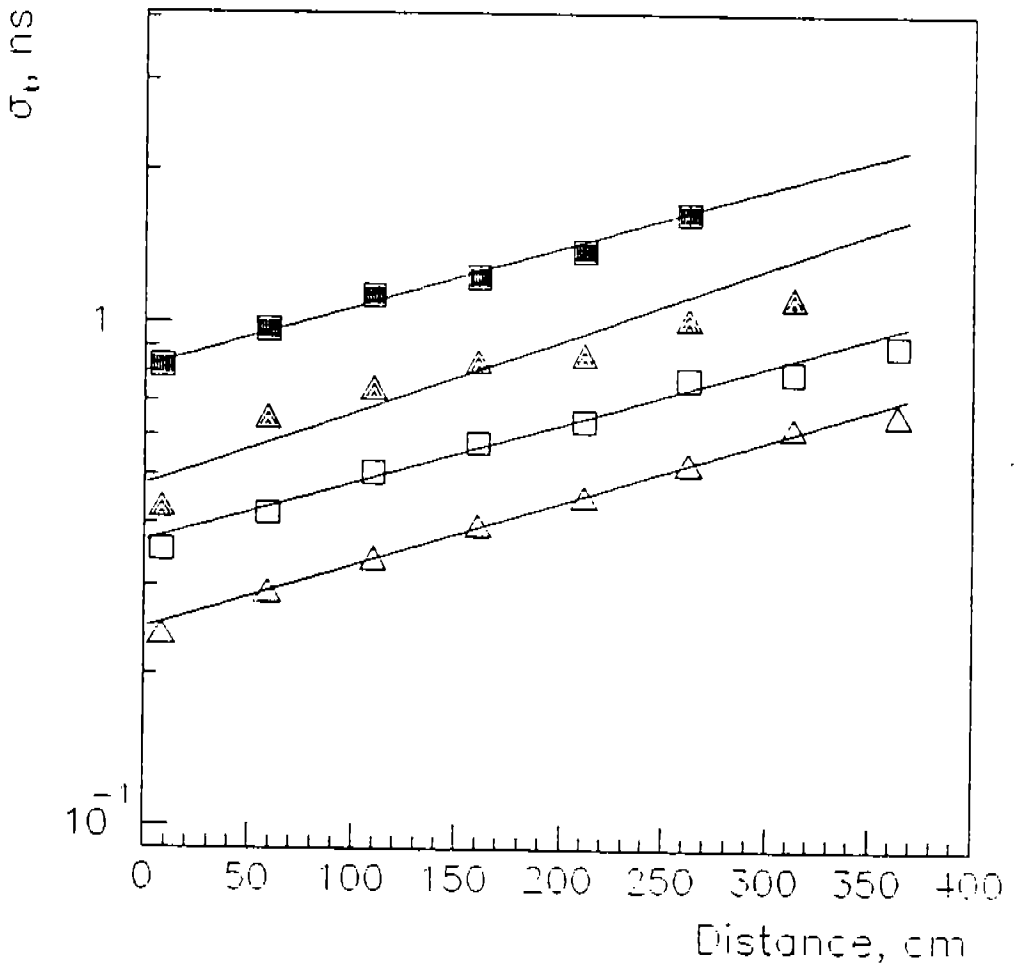

Figure 15

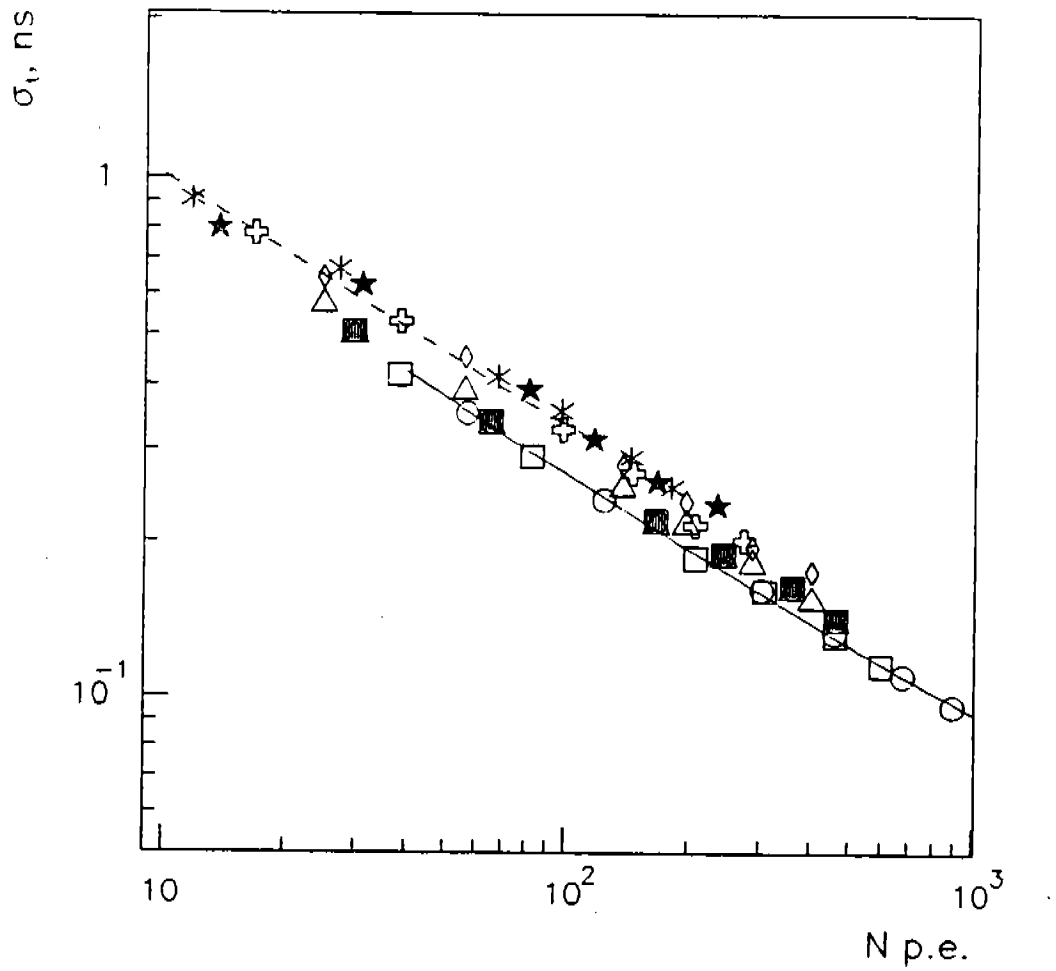

Figure 16

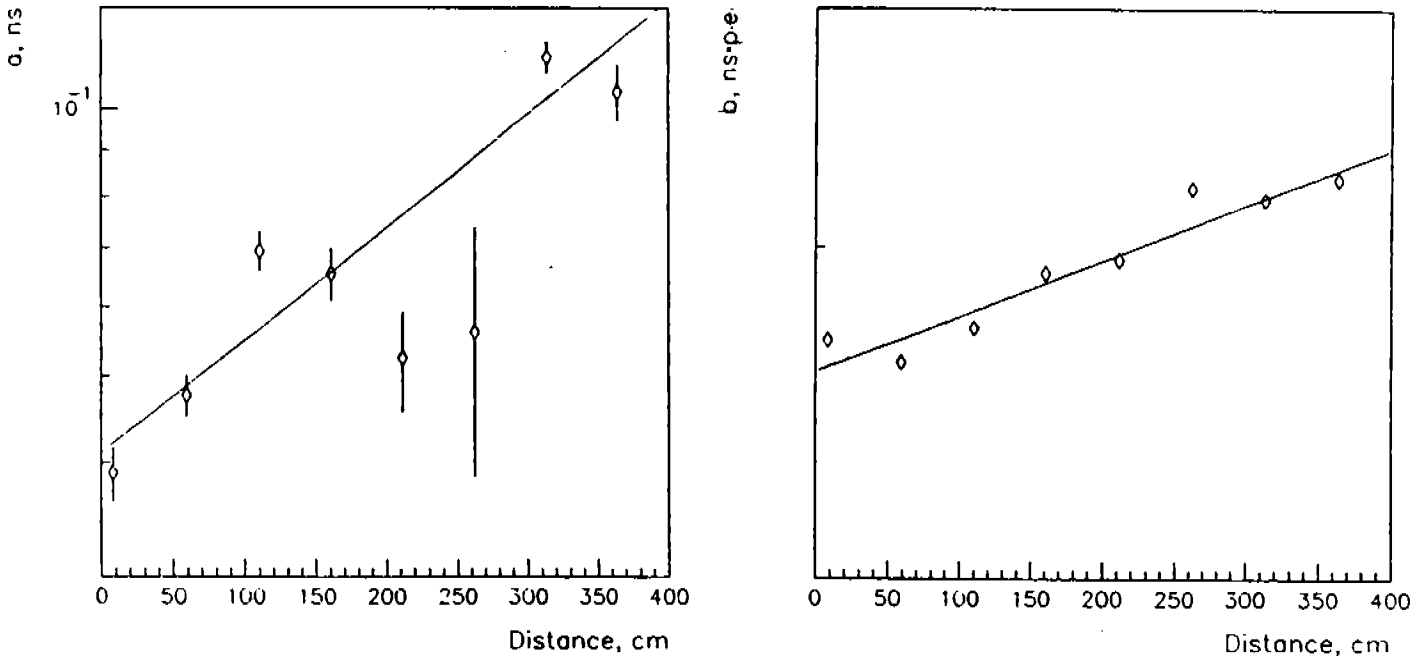

Figure 17

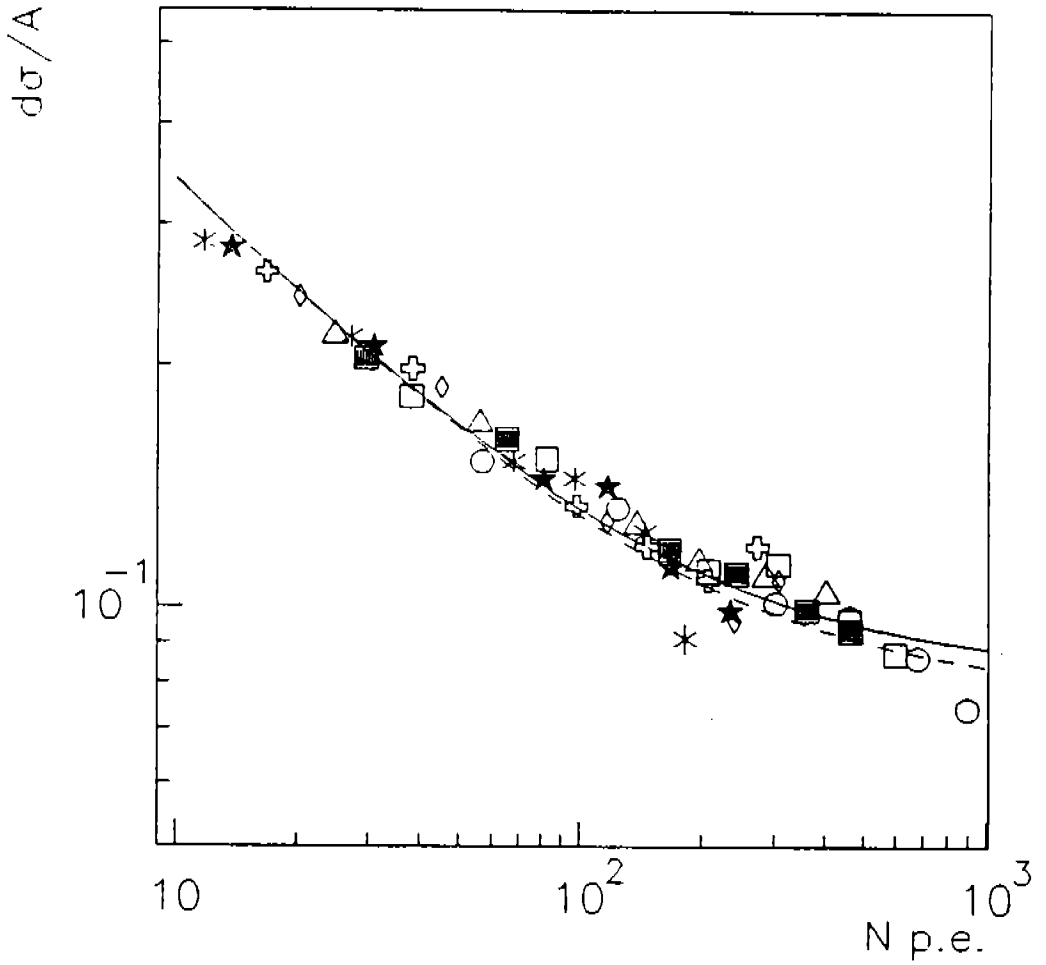

Figure 18

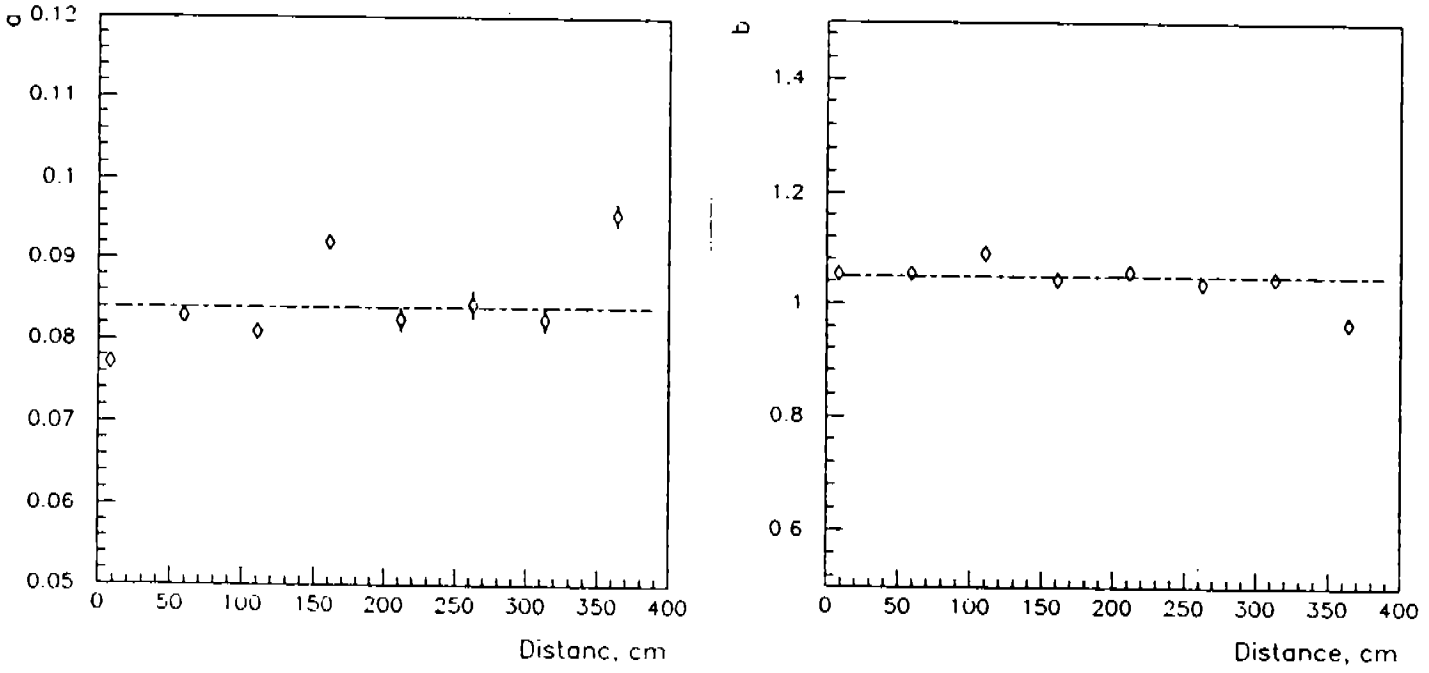

Picture 19